

ROTOR BLADE-VORTEX INTERACTION NOISE REDUCTION AND VIBRATION USING HIGHER HARMONIC CONTROL

Thomas F. Brooks and Earl R. Booth, Jr.
NASA Langley Research Center
Hampton, Virginia, U.S.A.

ABSTRACT

A rotor acoustics test was conducted to examine the use of higher harmonic control (HHC) of blade pitch to reduce blade-vortex interaction (BVI) noise. A dynamically scaled, four-bladed, articulated rotor model was tested in a heavy gas (Freon-12) medium in Langley's Transonic Dynamics Tunnel. Acoustic and vibration measurements were made for a large range of matched flight conditions where prescribed (open loop) HHC pitch schedules were superimposed on the normal (baseline) collective and cyclic trim pitch. A new sound power measurement technique was developed to take advantage of the reverberance in the hard walled tunnel. Special calibrations permit straightforward acoustic scaling of the results to those one would obtain in air. Quantitative sound power results are presented for a 4/rev (4P) collective pitch HHC. By comparing the results using 4P HHC to corresponding baseline (no HHC) conditions, significant mid-frequency noise reductions of 5-6 dB are found for low-speed descent conditions where BVI is most intense. For other flight conditions, noise is found to increase with the use of HHC. Low frequency loading noise, as well as fixed and rotating frame vibration levels, show increased levels.

SYMBOLS

a_0 speed of sound in test medium, ft/sec

C_T rotor thrust coefficient, thrust/ $\rho\pi R^2(\Omega R)^2$

F measured force component acting normal to shaft, Eq. (4), lb

f normal force at hub due to the application of HHC, Eq. (4), lb

f frequency, cyc/sec

f_{bp} blade passage frequency, number of blades $\times \Omega/2\pi$

K constant which includes control system masses, Eq. (4), lb sec²

M_T hover tip Mach number, $\Omega R/a_0$

nP n'th harmonic of rotor rotational period

R rotor radius, ft

SPL sound pressure level, pressure reference is 20 μ Pa

SWL sound power level, power reference is 10⁻¹² watt

α rotor tip path plane angle referenced to tunnel streamwise axis, deg

α' effective α corrected for closed-wall wind tunnel effect, deg

Γ tip vortex strength, ft²/sec

\ominus calculated "full-scale helicopter" flight descent angle, positive in descent, deg

θ pitch angle of blade at Ψ , deg

θ_C amplitude of higher harmonic pitch at Ψ_C , deg

μ advance ratio, tunnel flow velocity/ ΩR

ρ density of test medium, slug/ft³

Ψ blade azimuth angle, deg

Ψ_C blade azimuth angle selected for θ_C , see Fig. 5, deg

Ω rotor rotational speed, rad/sec

INTRODUCTION

Blade-vortex interaction (BVI) noise has for a number of years been an important topic of rotorcraft acoustics research. This impulsive type mid-frequency noise is due to blade interaction with shed vortices of preceding blades. A noise reduction concept is that decreases in blade lift, vortex strength, and/or increases

in blade-vortex displacements at the blade-vortex encounters should reduce the intensity of the interactions and thus noise (Ref. 1). An application of this idea is illustrated in Fig. 1, which shows blades undergoing higher harmonic pitch variations. The amplitude and phasing of such pitch controls would be expected to be important to the noise problem, as the strongest BVI occurrences are located within limited azimuth angle ranges, between approximately $\Psi=45^\circ$ and 75° in the first rotor quadrant (Ref. 2). Because of its significant potential, higher harmonic control (HHC) of blade pitch is a subject of interest for noise control where historically HHC has been studied as a means to reduce vibration levels (Ref. 3).

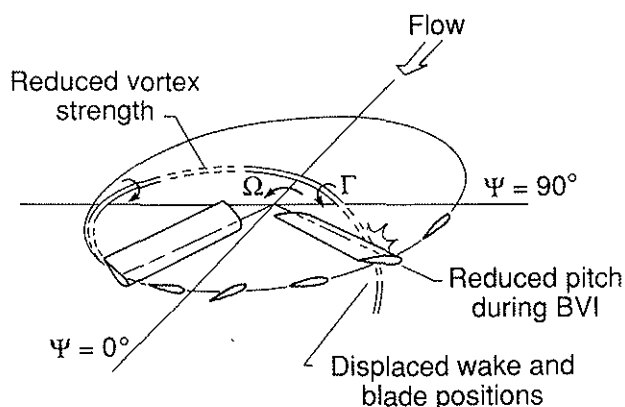


Fig. 1 Illustration of noise reduction concept.

In mid 1989, the initial findings from two independent research programs were reported (Refs. 4 and 5) on rotor tests designed to evaluate the noise reduction benefit of HHC. Reference 4, which is the forerunner to the present paper, reported that significant BVI noise reduction (4-5 dB) were found for low-speed descent conditions where BVI noise is normally most intense. The particular prescribed pitch schedule used for the HHC was a 4/rev (4P) collective pitch control. On the negative side, the use of HHC was found to increase low-frequency noise, as well as vibration levels. The results of Ref. 5 were quite consistent with those of Ref. 4. Although the number of flight conditions were limited in Ref. 5, three HHC pitch schedules (3P, 4P, and 5P) were examined. Each of these three produced similar BVI noise reductions and somewhat similar vibration results. Rotor performance/wake code calculations were reported for one of the flight conditions, which indicated that blade loading decreased and blade-vortex displacement increased at BVI locations for maximum BVI noise reduction, which would be consistent with the noise reduction concept mentioned previously. However, vortex strength was calculated to be increased.

This paper, in many respects, represents an expanded and more quantitative version of Ref. 4. Whereas Ref. 4 was based on on-line filtered levels from 3 test microphones, here the noise results are in terms of sound power spectra which were determined from 12 microphones, following extensive analytical and experimental calibrations. Also, the analysis is expanded to include low-frequency noise functional behavior and that of fixed and rotating frame vibratory system loads. The present results offer a more complete data base to assist in understanding the physics, evaluating the potential, and developing predictive capabilities for the use of HHC to reduce BVI noise.

This rotor test was designed to evaluate the noise reduction benefit of HHC. The test approach involves the measurement of noise and vibration with and without prescribed HHC pitch inputs superimposed on the normal cyclic trim pitch. Uniquely, the acoustic testing was conducted in a heavy gas (Freon-12) flow medium, rather than air, and the reverberant field of the hard wall tunnel test section was used to advantage by making acoustic measurements using a sound power determination approach.

EXPERIMENT

The test program was conducted in the Langley Transonic Dynamics Tunnel (TDT) using the Aeroelastic Rotor Experimental System (ARES). Fig. 2 shows the test set-up with in-flow microphones

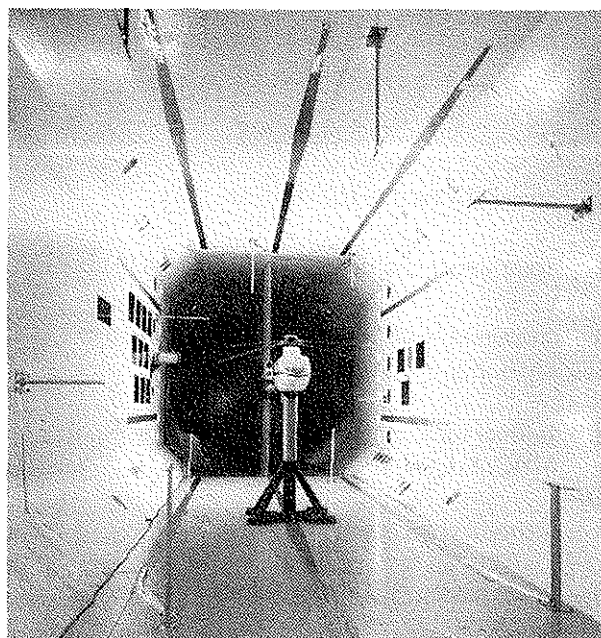


Fig. 2 Noise test set-up with microphones mounted upstream and downstream of the ARES model in the TDT.

mounted upstream and downstream of the rotor model in the test section. The test section is 16 ft. square with cropped corners. Either air or Freon-12 gas can be used as the test medium in the TDT. For this test, Freon-12 at a nominal density ρ of .0046 slug/ft³ (nominal pressure of .45 atmosphere) was used. The 110 in. diameter rotor, which is dynamically-scaled for Freon, has untwisted NACA 0012 section blades with a 4.24 in chord. The articulated flap and lead-lag hinges are offset 3 in. from the center of rotation. As a consequence of the Freon medium, test speeds (rotor and tunnel) are reduced, compared to what one would use in air, by the ratio of the speed of sound for Freon-12 and air, $(a_0)_{\text{freon}}/(a_0)_{\text{air}}=500/1130=.43$. This gives matched Mach number and advance ratio conditions at reduced frequency scales (Ref. 6).

Aeroacoustic Testing In Heavy Gas

Because this was the first aeroacoustic test to be conducted in a heavy gas medium, detailed acoustic calibrations were performed. To address microphone sensitivity questions for the Freon-12 medium, a special calibration was performed prior to the tunnel test. It was found that, for a pressure corresponding to tunnel test conditions, the microphones were found to have almost the same diaphragm sensitivity (within 0.2 dB) as air at one atmospheric pressure. As for microphone body diffraction effects on sensitivity, the acoustic wavelengths for identical frequencies in Freon-12 are smaller by the ratio of the speed of sound for Freon and air (.43 as indicated above). However, because of the lowered frequencies due the lowered rotor rpm in Freon, the acoustic wavelengths for the same rotor harmonics are the same for both air and Freon. Therefore, the microphone response in Freon at specific harmonics of the blade passage frequency, f_{bp} , is the same as if the test on this model had been conducted in air.

In the TDT, flow-noise calibrations were performed in both air and Freon. The results reinforced the conclusions of a scaling law analysis, based on fundamental aeroacoustic equations, that acoustic pressures are readily scaled between test media. One can show, following the same scaling logic developed in Ref. 7, that for matched Mach number rotor conditions, $(U/a_0)_{\text{h.g.}}=(U/a_0)_{\text{air}}$, that

$$\left(\frac{f}{a_0}\right)_{\text{h.g.}} = \left(\frac{f}{a_0}\right)_{\text{air}} \quad (1)$$

and

$$\left(\frac{p}{\rho a_0^2}\right)_{\text{h.g.}} = \left(\frac{p}{\rho a_0^2}\right)_{\text{air}} \quad (2)$$

The equations say that for a given microphone, rotor (or other source), and tunnel that the scaled noise is independent of medium (heavy gas, h.g., or air). In the analysis, it is assumed that all flow details and model dynamics are matched. The accuracy of this sweeping assumption depends on Reynolds number and other nondimensional parameter similarities—factors of common concern in wind tunnel testing. In this regard, with the noise data interpretation being straightforward, a net test advantage is found by using a heavy gas medium for this test because the rotor is dynamically scaled and the Reynolds numbers are higher (by 17 percent for this test) compared to air.

Sound Power Measurement Method

Because of the reverberant character of the TDT test section, it was decided not to attempt directivity measurements but to employ a sound power measurement method that would take advantage of the reverberance. In addition to being a practical approach for the hard walled tunnel, the method is attractive because it produces a single quantitative spectrum (obtained from spatial averaging) for each test condition making it convenient for data interpretation.

Twelve one-quarter inch diameter B&K pressure type microphones, six upstream and six downstream of the rotor model, were used to make the noise measurements. Figure 2 shows the microphones fitted with nose cones and mounted in vibration isolated streamlined stands. The microphones are placed 13 and 16 ft. from the rotor model center, away from the nearfield of the rotor noise sources. The normally open slots in the tunnel wall were covered to further enhance test section reverberance, thereby reducing statistical variance of noise measured between microphones.

The sound power calibration was a multi-phase experimental-theoretical effort, with the goal being to determine the relationship between the microphone measurements and the sound power emitted by the model in the tunnel. Experimentally, two calibrators were used. One was a commercial B&K reference sound source of known broadband characteristics. The other was a special calibrator, with a small source region and a reference microphone to monitor its output, which could be tested in tunnel flow for both air and freon. In Fig. 3, this is shown mounted from the tunnel wall, positioned in the nominal rotor advancing-side noise region (rotor was removed). Tests performed in air in a quality reverberant chamber and in

the TDT produced good quantitative comparison between the results for the two sources. A key calibration result is shown in Fig. 4 for the Freon test environment. It is the spectral transfer function (TF) relating sound power level (SWL) to the average sound pressure level (SPL_{avg}) for the 12 microphones. Good agreement is seen with theory (discussed below) between about 0.7 to 3 kHz, where the calibrator results are believed to be accurate. At lower frequencies the calibrator signal-to-noise was poor and at higher frequencies the source output was not clearly defined by the reference microphone. The effect of tunnel velocity on the transfer function of Fig. 4 was found to be minimal, as was supported by theory for velocities below $M=0.2$.

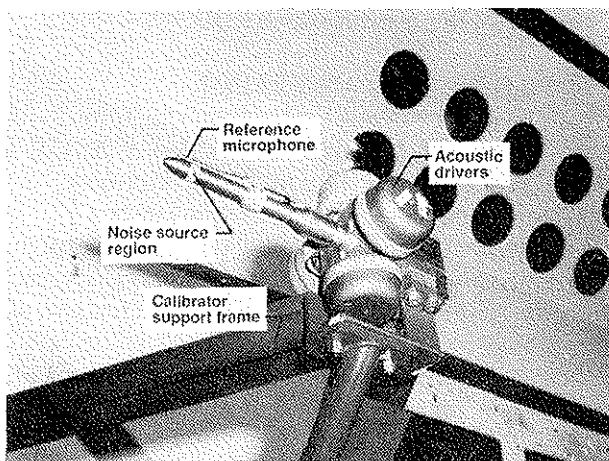


Fig. 3 Sound power calibrator mounted from TDT wall.

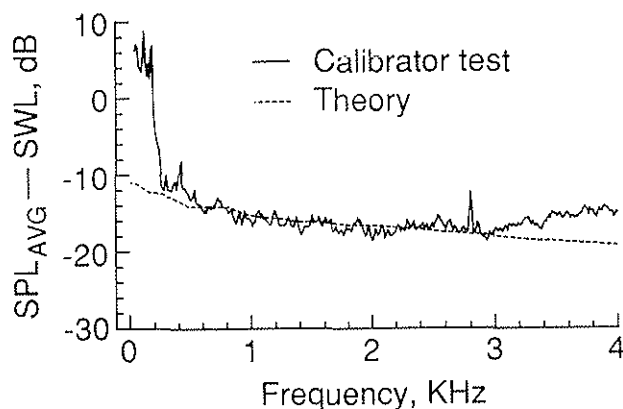


Fig. 4 Transfer function of the average SPL for microphones in the TDT to the SWL of a noise source in Freon-12 at 0.45 atmospheric pressure. Tunnel velocity is zero.

A theoretical model helped establish the initial positioning of the microphones in the TDT, provided an evaluation of the calibrator TF results, and extended

the useful range of the results. The model employs a simple monopole source and dipole sources, of arbitrary orientation, positioned in the rotor region of a 16 ft.-square duct (TDT cropped corners were not modeled). The wall reflections (reverberances) are modeled by a system of mirror images (100 x 100 images used). Tunnel flow convection effects on source directivity and propagation are included. Test medium sound absorption was modeled in a manner consistent with that of Ref.8. The values of absorption coefficients were known for air (relative humidity ≥ 50 percent) and worked well in the modeling. For Freon-12, values somewhat larger than those of air were used and produced good results. The theoretical TF in Fig. 4 is for an incoherent (or white noise) simple source. Attenuation due to the use of nose cones on the microphones in a reverberant field has been taken into account. The use of arbitrarily oriented dipoles, rather than monopoles, give the same TF within 1 dB (except for dipoles aligned almost parallel to the test section centerline—not a characteristic of the rotor sources of interest here). The use in the model of a coherent (phase-locked) source would render predictions more similar in appearance to the calibrator result, with fluctuations very similar in amplitude (± 1 dB) and frequency spacing. But since fluctuation peak and valley locations were found to depend on source type and orientation, which is not known for the rotor sources, we use the smooth theory result of Fig. 4 to obtain power spectra for all rotor test results. Based on these concerns, the SWL accuracy should be within 1 dB for each harmonic. A 1.5 - 2 dB accuracy is suggested for the first few low-frequency harmonics where the loading noise source, which is acoustically noncompact and thus is not accounted for in the calibrations, dominates. Importantly, however, the variability error between rotor cases for particular harmonics of all frequencies should be less than 1 dB. For SWL spectra obtained in Freon, one can obtain the SWL spectral for a rotor test conducted in air by

$$SWL(f)_{air} = SWL(f)_{freon} + 20 \log \left[\frac{(\rho a_0^3)_{air}}{(\rho a_0^3)_{freon}} \right] \quad (3)$$

where the frequencies f , and bandwidths Δf , are related through Eq. (1).

Rotor Operation

Pitch motion is applied to the rotor blades through swashplate motions due to three hydraulic actuators. For this four-bladed rotor, the higher harmonic pitch is achieved by superimposing 4/rev (4P) swashplate motion upon basic fixed swashplate collective and

cyclic (1P) flight control inputs. Collective 4P pitch motion (all 4 blades pitching the same way simultaneously) is possible, as well as pitch schedules containing 3P, 4P, and 5P pitch harmonic components, through proper phasing the 4P inputs (Ref. 3, 9). For this test, a specially developed computer-based open-loop control system was used to superimpose the HHC signals on the ARES control system. The pitch motion achieved, as well as the test procedure, can be described with the aid of Fig. 5 which shows blade pitch angle data versus blade azimuth angle Ψ for a specific "flight" condition. For a given advance ratio μ and tip path plane angle α , the mean collective (6.5°, for the case shown) required to achieve the prescribed C_T and the basic 1P (3.8°) pitch control for zero flapping trim, with respect to the rotor shaft, were attained. Once performance, and acoustic data were taken for this baseline case, prescribed HHC pitch was superimposed to obtain a deflection of θ_c at azimuth angle Ψ_c and data again taken. For some rotor conditions, small adjustments were necessary in the mean collective and cyclic to maintain identical C_T and

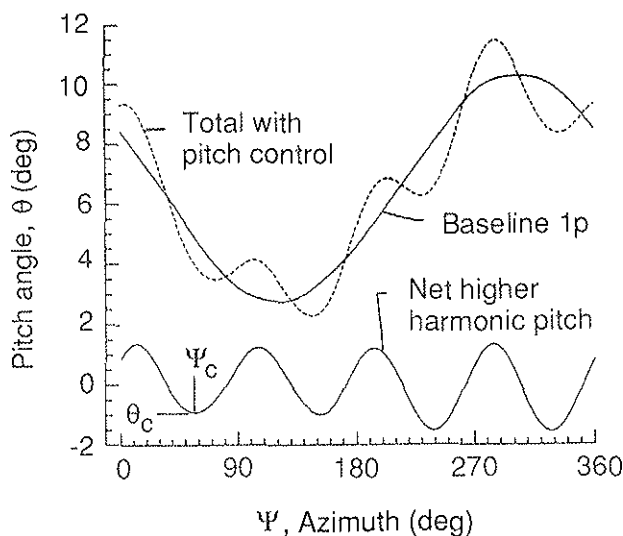


Fig. 5 Blade pitch angle θ versus azimuth Ψ for $\mu = .266$ and $\alpha = 0^\circ$. Pitch control is 4P collective with $\theta_c = -1.2^\circ$ at $\Psi_c = 58^\circ$.

trim flight conditions, although none were needed for the case of Fig. 5. The higher harmonic pitch portion (obtained by subtraction of the total from the baseline case) is seen at the bottom of the figure. The net pitch is seen not to be purely a 4P collective, but contains other harmonics due to normally occurring pitch-flap and pitch-lag couplings. For the 4P noise data shown in this report, HHC amplitude θ_c and azimuthal angle Ψ_c in the first quadrant ($0 \leq \Psi_c < 90^\circ$) are defined from the 4P component of the pitch motion FFT analyses.

Reference 4 specified only the nominal control-system-command values of θ_c and Ψ_c .

The rotor was tested over a broad range of operating conditions where the rotor thrust coefficient C_T was maintained at 0.005. Rotor advance ratios μ less than 0.11 were not possible due to wind tunnel minimum operating speed limitations. The rotor rotational speed was held constant at $\Omega=650$ rpm (the hover tip Mach number was nominally $M_T=0.62$). Specific test "flight" conditions were defined based on the tunnel referenced tip path plane angle α and the advance ratio μ at the specified C_T . For the data presented, the tip path angles were corrected (Ref. 10) to account for the closed wall wind tunnel effects to obtain equivalent freestream α' values. Also, in order to interpret the noise results in terms of full scale flight conditions, equivalent flyover descent angles Θ were calculated (Ref. 11) based on fuselage-rotor drag of a MBB BO-105.

NOISE RESULTS

The sound power level (SWL) spectra are determined from mean-square averaging the SPL spectra of all 12 microphones and employing the theoretical transfer function of Fig. 4. The SPL spectra, bandwidth = $f_{bp}/4=11$ Hz, were determined from FFT's keyed to the one-per-rev of the acoustic pressure time histories. The number of averages was 250.

In this section, the spectral and time history noise characteristics are examined. Also, noise levels, representing the low and mid-frequency portions respectively of the SWL spectra, are presented for different flight and HHC conditions. The low-frequency levels are obtained by integrating or band-pass-filtering from zero to $5.5 f_{bp}$, which are taken to represent the contributions from harmonic loading noise. The mid-frequency levels are obtained by band-pass-filtering from 5.5 to $40.5 f_{bp}$. These mid-frequency levels are dominated by impulsive BVI noise contributions for rotor conditions where BVI occurs. Where BVI noise is not prevalent, the mid frequency levels are due to the higher frequency harmonics of loading noise, as well as broadband noise from blade-turbulent wake interactions (BWI), Ref. 11.

Noise Characteristics

Figure 6 shows sound power level (SWL) spectra for a test condition where mid-frequency BVI noise was reduced by the use of 4P HHC, but low-frequency noise was found to increase. This spectral behavior is typical over the range of low-speed descent conditions where HHC proved beneficial for BVI noise reduction. At an advance ratio of $\mu=.11$ and a helicopter descent angle of

$\Theta=10.5^\circ$ (tip path plane angles α and α' are shown in parentheses), the rotor wake should be at or somewhat above the plane of the rotor. The baseline (no HHC) spectrum shows low-frequency harmonic noise, due steady and unsteady blade loading, to be dominant through at least the fourth harmonic ($4 f_{bp}$). At higher frequencies, BVI noise dominates. The 4P HHC which is used has a peak pitch amplitude of $\theta_c=-1.2^\circ$ at an azimuth angle of $\Psi_c=60^\circ$. With HHC, the BVI noise is reduced by 4.5 dB in terms of the mid-frequency integrated levels mentioned above, whereas the low-frequency integrated levels increased by 6.5 dB. The flight condition is not where the maximum BVI noise reduction was found in the test. At a less steep descent rate of 8.5° , a reduction of 5.6 dB was measured.

It is important to note, that on the subjective A-weighted dB scale, the low frequency noise (even with its hefty increases using HHC) is inconsequential compared to the BVI noise dominated mid-frequency

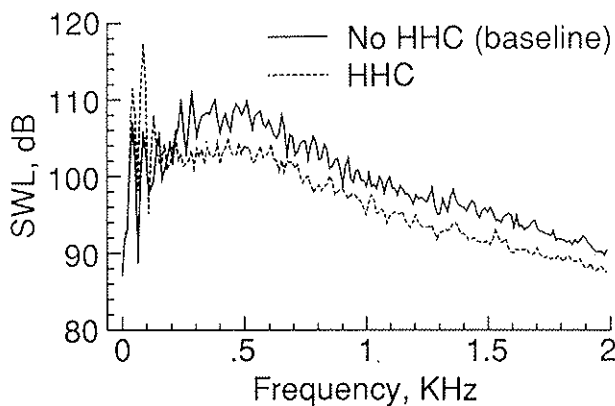


Fig. 6 Sound power spectral comparison showing the effect of the use of HHC for $\mu=0.11$ and $\Theta = 10.5^\circ$ ($\alpha = 8.0^\circ$, $\alpha' = 9.5^\circ$). HHC amplitude is $\theta_c = -1.2^\circ$ at $\Psi_c=60^\circ$. Bandwidth is 11 Hz.

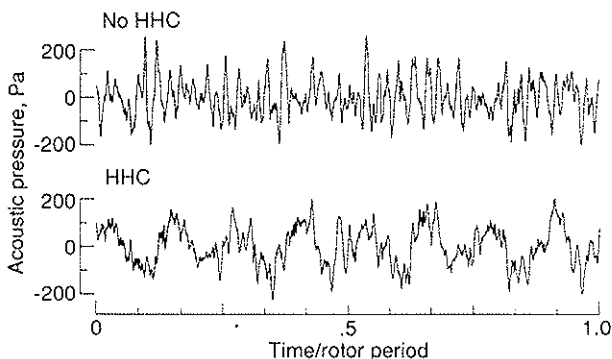
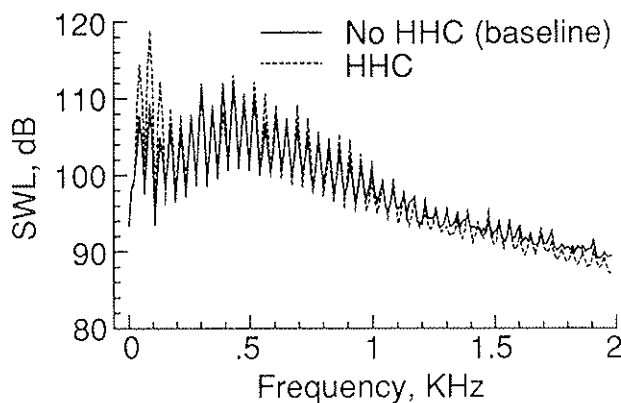


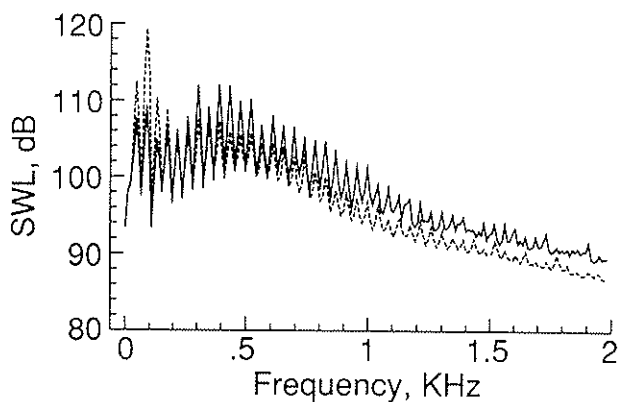
Fig. 7 Microphone signal time histories showing the effect of the use of HHC for the case of Fig. 6.

noise. For example, the second harmonic at $2 f_{bp}=88$ Hz (in full scale this would be 64 Hz or lower) must be attenuated by about 25 dB on the dBA scale compared in importance to the mid-frequency harmonics.

The change in character of the rotor noise sources with the use of HHC can be observed through the instantaneous acoustic pressure time histories. These, given in Fig. 7, correspond to the cases of Fig. 6. The microphone is forward of the rotor on the advancing side, although any microphone gives very similar results because of spatial uniformity from the many wall reflections contributing to the acoustic pressure in the tunnel. One sees, with no HHC, that the noise is dominated by impulsive BVI occurrences. The use of HHC for this case diminishes the BVI levels and, perhaps, the number of occurrences. A large increase in



(a) HHC $\theta_c = -1.3^\circ$ at $\Psi_c = 14^\circ$



(b) HHC $\theta_c = -1.3^\circ$ at $\Psi_c = 57^\circ$

Fig. 8 Sound power spectral comparison showing the effect of HHC phase for $\mu = 0.2$ and $\Theta = 5.9^\circ$ ($\alpha = 2.0^\circ$, $\alpha' = 2.4^\circ$). Bandwidth is 11 Hz.

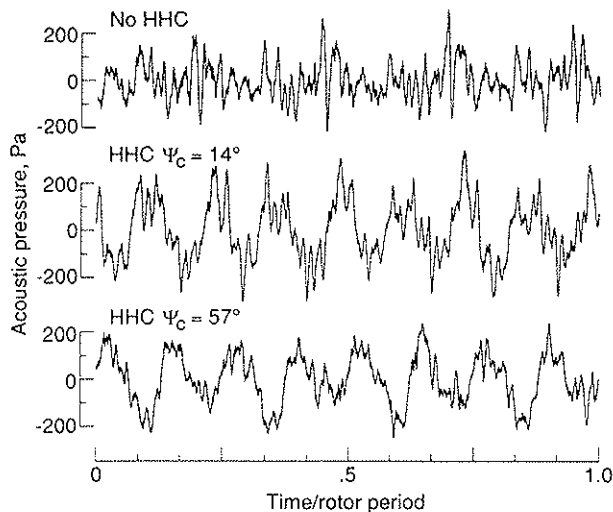
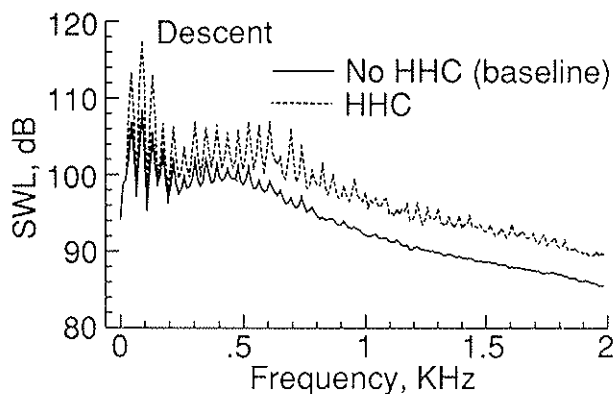
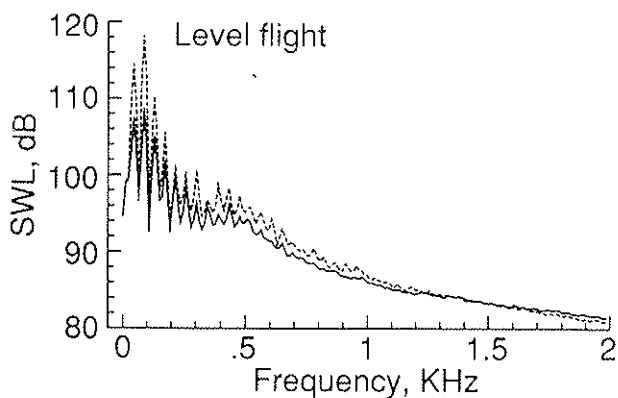


Fig. 9 Microphone signal time histories showing the effect of HHC phase for cases of Fig. 8.

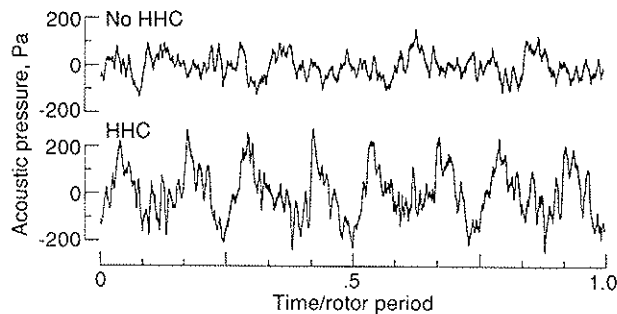


(a) Descent angle $\Theta = 9.9^\circ$ ($\alpha = 6.0^\circ$, $\alpha' = 6.4^\circ$)

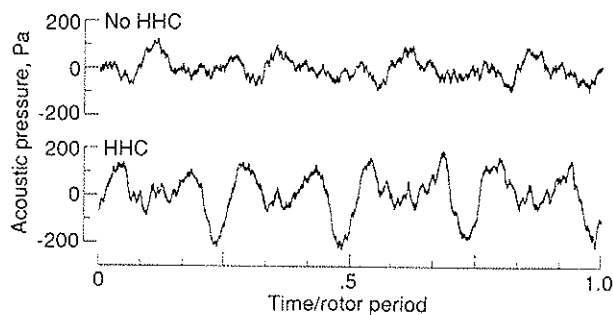


(b) Descent angle $\Theta = 0.0$ ($\alpha = -4.0^\circ$, $\alpha' = -3.6^\circ$)

Fig. 10 Sound power spectral comparison showing the effect of rotor descent angle on the use of HHC for $\mu = 0.2$. HHC $\theta_c = -1.2^\circ$ at $\Psi_c = 60^\circ$. Bandwidth is 11 Hz.



(a) Descent angle $\Theta = 9.9^\circ$



(b) Descent angle $\Theta = 0.0^\circ$

Fig. 11 Microphone signal time histories showing the effect of rotor descent on the use of HHC for the cases of Fig. 10.

the eight-per-rev harmonic is clearly seen, which corresponds to the $2 f_{bp}$ component in Fig. 6.

The effect of 4P HHC phase on the noise can be examined through Fig. 8, where spectra for amplitudes of $\theta_c = -1.3$ at different Ψ_c azimuth angles are shown. At this moderate speed of $\mu = 0.2$ at a descent of $\Theta = 5.9^\circ$, the rotor plane should be operating in or about the wake. The use of $\Psi_c = 57^\circ$ reduces the mid-frequency spectral levels (3 dB in terms of integrated level), whereas $\Psi_c = 14^\circ$ has little effect. Low-frequency integrated levels are increased for both by almost 7 dB. Instantaneous pressure time histories, corresponding to Fig. 8, is shown in Fig. 9. The BVI impulsive character is seen not to be affected for $\Psi_c = 14^\circ$, whereas it is diminished for $\Psi_c = 57^\circ$. The phase of the eight-per-rev harmonic ($2f_{bp}$) appears to follow the Ψ_c phase. This suggests, as would be expected, that the higher harmonics of blade loading, which produces the low-frequency noise, simply rotates (shifts azimuthally) with the HHC phasing.

The influence on noise of helicopter descent angle Θ , at moderate speed $\mu = 0.2$, is illustrated in Fig. 10 for

a HHC amplitude of $\theta_c = -1.2^\circ$ at $\Psi_c = 60^\circ$. At $\Theta = 9.9^\circ$, where, for this speed the wake should be substantially above the rotor plane, the mid-frequency integrated noise increases 4.2 dB with HHC. At level flight, $\Theta = 0.0^\circ$, the level increases 1.8 dB. For both cases, the integrated low-frequency levels increase 7 dB. The corresponding time histories are shown in Fig. 11. For the steep descent angle, $\Theta = 9.9^\circ$, the comparisons show

quite interestingly that the use of HHC apparently incur new BVI occurrences and noise. This tends to confirm that at least part of the fundamental effect of HHC on BVI noise is due to tip-vortex wake trajectory and/or blade position changes. For level flight, $\Theta = 0.0^\circ$, little BVI noise is in evidence with or without HHC. The mid frequency range for this case is dominated by relatively non-impulsive loading noise.

BVI (mid frequency) Noise Levels

To more clearly show how operational pitch control variations affect rotor noise, the low and mid-frequency integrated noise levels were examined separately. For the important mid frequencies (5.5 to 40.5 f_{bp}), noise levels are presented in Fig. 12 for 9 different flight conditions, where the rotor operated at baseline (without HHC) and also where 4P HHC was used at different amplitudes and phases. Figures 12(a)-(c) present levels for steep descent angles where the rotor wakes are primarily above the plane of the rotor. Part (a) is for a advance ratio of $\mu = 0.166$ and helicopter descent angle of $\Theta = 9.1^\circ$. The noise levels are plotted versus the 4P HHC azimuth angle Ψ_c corresponding to the minimum peak amplitude θ_c . The amplitudes for the test cases varied somewhat with rotor conditions (± 10 percent), but only the nominal values of $\theta_c = -0.6^\circ$ and -1.2° are specified in the figure, as indicated by symbols. The angles Ψ_c are accurately plotted. The baseline case ($\theta_c = 0^\circ$) is shown positioned at the $\Psi_c = 0^\circ$ plot location, for convenience. The noise results represented by solid symbols are repeat test points to be subsequently discussed. It is seen, for the Fig. 12(a) flight case, that the noise level generally increases above the baseline condition for the HHC conditions shown, especially near $\Psi_c = 0^\circ$ (or 90°) and 60° . The larger control pitch of $\theta_c = -1.2^\circ$ produced the larger noise increases. Similar trends are seen for Fig. 12(b) and (c), where the descent angles are also steep. The noise character of the baseline cases at these angles was not substantially impulsive, however, the impulsiveness (BVI) increased for a number of HHC cases, as evidenced in the steep descent angle case of Fig. 11(a).

Fig. 12(d)-(f) are for descent angles and speeds where the rotor generally operates in or about its own wake. BVI noise is expected to be most intense for these cases and, indeed, the baseline cases have higher levels than those at steeper angles, especially at lower μ . The impulsive character of the noise is seen in the time histories of Fig. 9, which corresponds to cases of Fig. 12(e). The use of 4P HHC is seen to reduce the noise for a range of azimuth control angles for the lower μ values. The greater pitch amplitude of $\theta_c = -1.2^\circ$ is seen to be most effective at the lowest μ

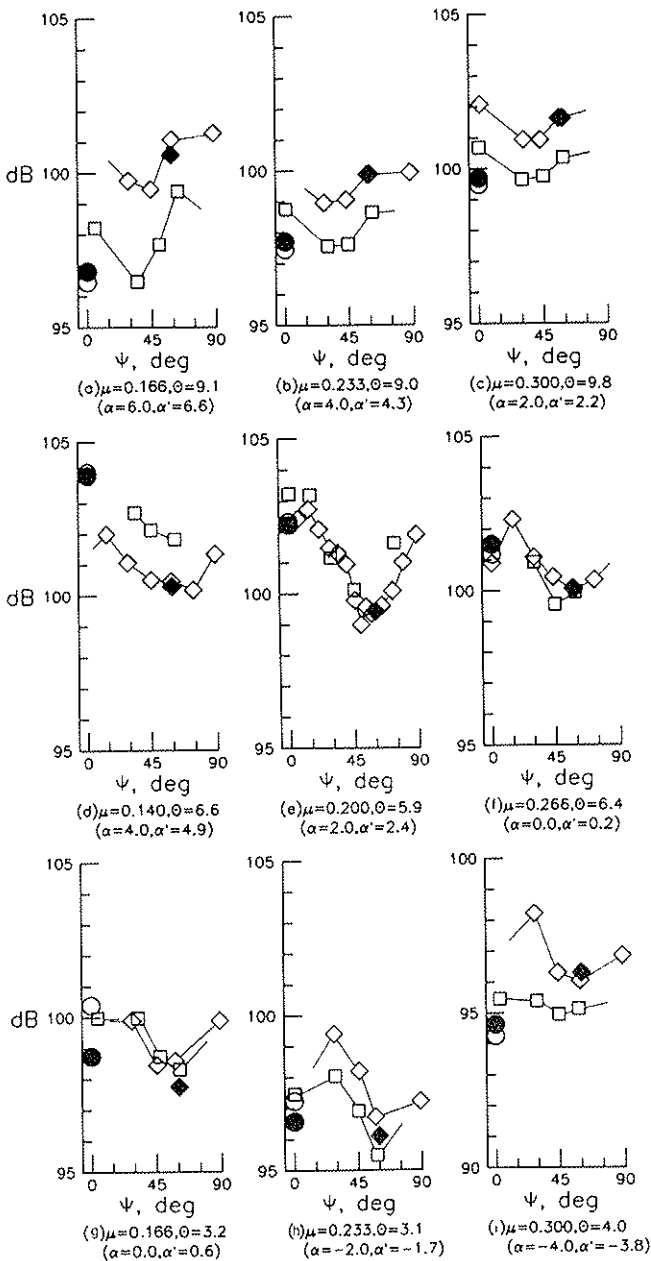


Fig. 12 Mid-frequency (5.5 to 40.5 f_{bp}) SWL (dB) variations with different 4P HHC amplitudes θ_c and azimuth Ψ_c . Symbols are for $\theta_c = 0^\circ$ (baseline), \circ ; for $\theta_c = -0.6^\circ$ (nominal), \square ; and for $\theta_c = -1.2^\circ$ (nom.), \diamond . Solid symbols are repeat cases.

values of .14 and .20, while the smaller $\theta_c = -.6^\circ$ is more effective at the somewhat higher $\mu = .266$ value. Note that the azimuth range where reductions occur, roughly between $\Psi = 45^\circ$ and 75° , correspond to the expected BVI locations (Ref. 2). This is consistent with the hypothesis that reductions in blade loading in the vicinity of BVI occurrences should reduce BVI noise. It can also be consistent with idea of reductions occurring due to wake trajectory and blade positioning changes with HHC application.

Fig. 12 (g)-(i) are for mild descent angles where the wake generally lies below the rotor. At the lower μ value of Fig. 12(g), the 4P HHC is seen to reduce noise using both $\theta_c = -.6^\circ$ and -1.2° . For the higher advance ratio of Fig. 12(h), $\theta_c = -.6^\circ$ is more effective. No net benefit is seen for pitch control in Fig. 12(i) for $\mu = .3$.

A portion of the test was directed at more clearly defining flight regimes where HHC can be used to reduce BVI noise. Fig. 13 shows, for the baseline (no control) case, a contour map of the mid-frequency noise levels for a broad range of scaled descent angles, Θ , and advance ratios, μ . A contouring program was used with measured levels at the test grid points indicated. Some test grid points are overlaid by letters to

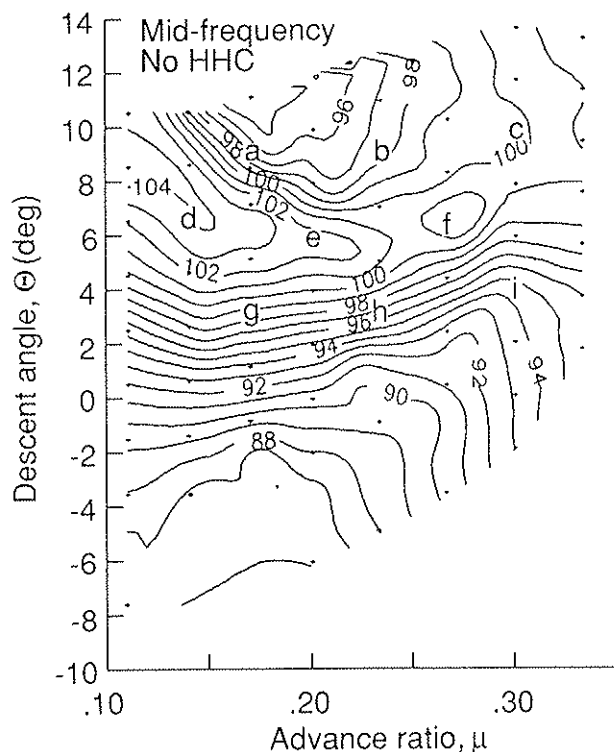


Fig. 13 Mid-frequency SWL (dB) contours versus flight condition for the baseline (no control) case. Contours based on values at grid points. Letters correspond to parts of Fig. 12.

correspond to the parts of Fig. 12. For reference, the noise levels determined during this part of the test are shown in Fig. 12 by the solid symbols. These are seen to be matched generally within one dB to the corresponding open symbols, which demonstrates the degree of repeatability. The BVI noise is seen to be most intense at lower speed and descent angles corresponding to normal landing approach for helicopters. The tunnel limitation, which prevented acquisition of data at advance ratios below $\mu = .11$, is unfortunate because of the importance of BVI noise at low μ . The intense BVI impulsive noise lies in a region which is approximately centered about $\Theta = 9^\circ$ at $\mu = .11$ and ranges to $\Theta = 6^\circ$ from about $\mu = .15$ to almost $\mu = .3$. The flight conditions of Figs 12(d)-(f) are positioned in this region, whereas the other points are seen to border it. The very steep descent, level, and climb flight regimes are dominated by non-impulsive loading and broadband noise in the mid frequency range.

The flight matrix of Fig. 13 was also conducted for a 4P HHC of $\theta_c = -1.2^\circ$ and $\Psi_c = 60^\circ$ (nominal values). While this pitch is seen in Fig. 12 to not always be optimum, it appears to give representative noise reductions for rotor conditions where reductions were found. Fig. 14 shows the contour plot for the resultant

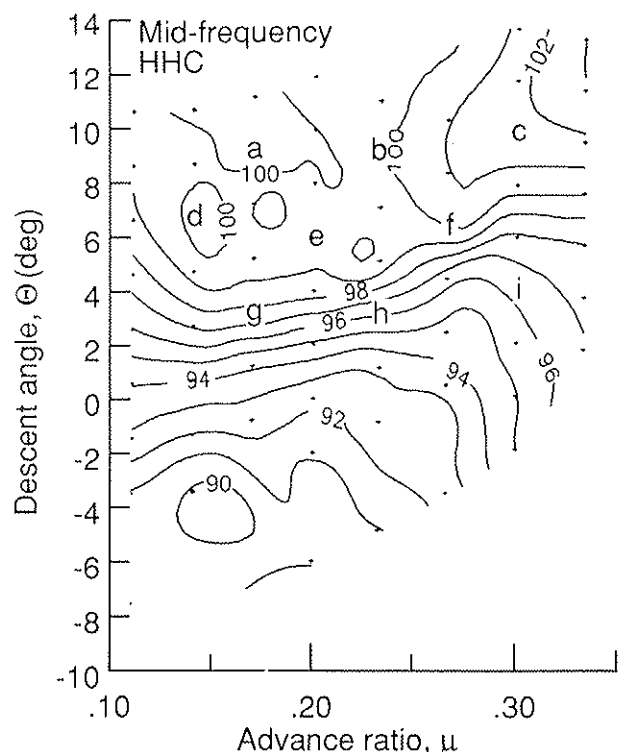


Fig. 14 Mid-frequency SWL (dB) contours versus flight condition for 4P HHC $\theta_c = -1.2^\circ$ and $\Psi_c = 60^\circ$ nominal case. Letters correspond to parts of Fig. 12.

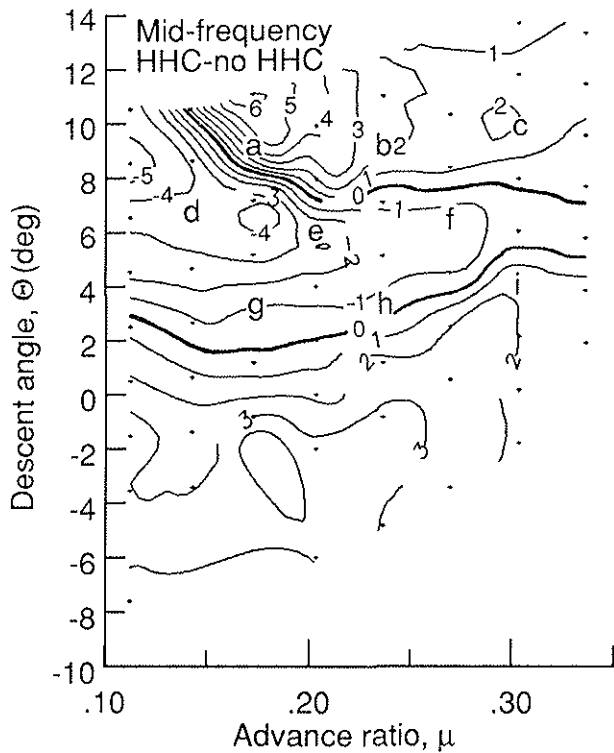


Fig. 15 Mid-frequency level (dB) differences between the HHC case of Fig. 14 and the baseline case of Fig. 13. Negative values show noise reductions for HHC case. Letters correspond to parts of Fig. 12.

levels. The effect on the noise is dramatic since the particularly intense BVI noise region is eliminated. Fig. 15 shows the relative change between the levels of Fig. 13 and that of Fig. 14. Noise reduction (negative level change) is seen limited to the landing approach flight regime where BVI noise is most important. The maximum mid frequency reduction found was 5.6 dB, at $\Theta=8.5^\circ$ and $\mu=.11$. Noise tends to increase where BVI noise is not dominant for baseline conditions; that is, for climb, level flight, steep descent, and high speed flight for all angles. The levels particularly increase for steep descent at low speeds (top of the figure), an indication that BVI occurrences can shift to different flight regimes with the use of HHC. As mentioned, the particular 4P HHC amplitude and phase used is not always optimum. Based on the discussion of Fig. 12, the noise reduction region could be expanded for 4P HHC over that shown by employing less amplitude in the outer fringes of the region.

Loading (low frequency) Noise Levels

As previously indicated, the low-frequency levels are not important from a subjective A-weighted measure in comparison to the mid frequencies. This fact gives a justification for concentrating on the mid

frequencies in the question of the use of HHC for noise reduction. However, low-frequency level increases are not desirable and the subject is dealt with in this section.

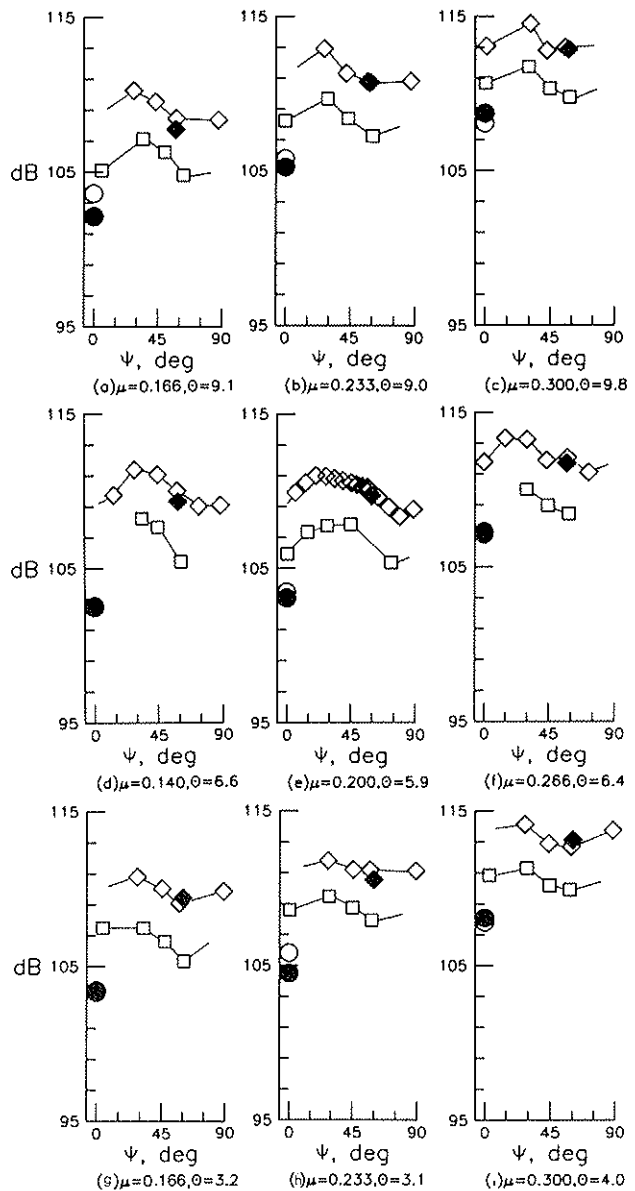


Fig. 16 Low-frequency (zero to 5.5 fbp) SWL (dB) variations with different 4P HHC amplitudes and azimuth phases. Symbol key as in Fig. 12.

In the format of Fig. 12, for the identical operational cases, Fig. 16 shows the low-frequency (zero to 5.5 fbp) integrated noise levels. Unlike mid-frequency noise, the low-frequency noise functional dependence on the 4P HHC amplitudes θ_c and azimuth angles Ψ_c is seen to be nearly independent of flight condition. Although all levels increase (rather uniformly) with increases in μ , there is little dependence on descent angle Θ . For the $\theta_c \sim 1.2^\circ$

amplitudes, the levels increase about 7 dB for $\Psi_c \sim 30^\circ$ azimuth. But, at about $\Psi_c = 60^\circ$ to 75° where BVI noise has been found to be reduced, the low frequency levels increase 6 dB or less which is relatively fortunate. These level increases are 3-4 dB lower for the smaller $\theta_c \sim .6^\circ$ amplitudes.

VIBRATORY LOADS

The practicality of implementing specific HHC for BVI noise reduction depends in part on the accompanying vibratory loads. Two measures of vibration loads are examined. One is the fluctuating normal force acting through the hub in the fixed system. The other is the flapwise bending moment at an inboard station of a rotating blade.

Fixed system loads were measured by a six-component balance mounted below the model base. It was desired to examine the 4P component of the normal force, which acts in line with the shaft axis. Analysis of the data base revealed that the measured normal force component for a HHC case, $(F_{4P})_{HHC}$, appeared to follow

$$(F_{4P})_{HHC} = (F_{4P})_{No\ HHC} + K(\ddot{\theta}_{4P})_{HHC} + (f_{4P})_{HHC} \quad (4)$$

where $(F_{4P})_{No\ HHC}$ is the measured value for the rotor operating at baseline (No HHC) conditions. The force terms are complex, having amplitude and phase. The force term (f_{4P}) is that due to the aerodynamic and aeroelastic effects of the use of HHC. The term $K(\ddot{\theta})_{4P}$ is the inertial force due to the accelerating masses of the swashplate, blade-root hardware, actuator pistons, and other control hardware used to produce the HHC pitch motion. The inertial term is the dominant contributor to the force measurement during the HHC for the ARES. Because the ARES test bed control hardware is not scaled in size to any helicopter, the inertial force component is extraneous for present purposes. Therefore, the inertial term was subtracted vectorially for each rotor test condition, which renders the net forces acting at the hub, $(F_{4P})_{No\ HHC} + (f_{4P})_{HHC}$. The value of K was equated to the component of force found to remain in-phase with $\ddot{\theta}_{4P}$ over all Ψ_c values examined. This was believed preferable to the determination of K from calibration testing, which was conducted without blades as part of the test program. There was uncertainty in the relevance of that calibration data, because the balance was unloaded and there was not a pertinent dynamic calibration to equate the results to a loaded condition.

From the above analysis of the data, Fig. 17 presents the 4P normal hub force amplitude versus control system amplitude and phase in the same format as Figs. 12 and 16. The force should represent that due only to aerodynamic and aeroelastic effects with and without 4P HHC, independent of control system inertial effects. Figures 17(d), (e), and (f), unfortunately, lack much of the HHC data because of the loss of a data channel during a portion of the test. The data presented, however, is sufficient to conclude that, in general, the vibratory forces tend to increase at

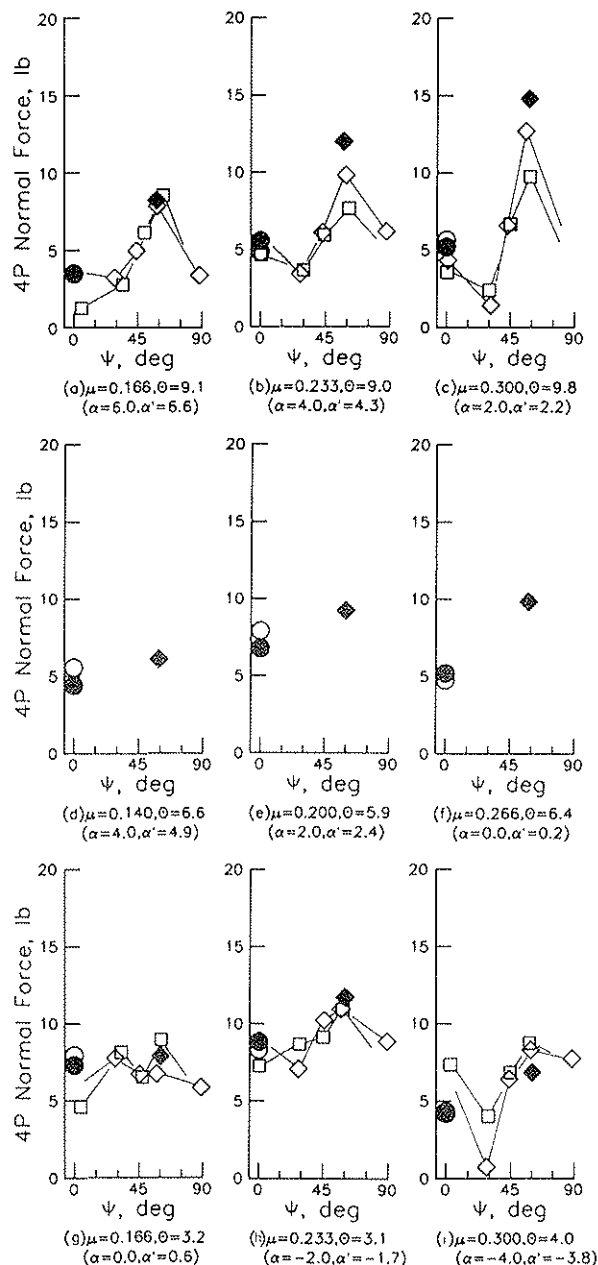


Fig. 17 4P normal (hub) force amplitude variation with different 4P HHC amplitudes and azimuth phases. Swashplate inertia forces removed. Symbol key as in Fig. 12.

Ψ_c values of about 60° and decrease at about 30° . This is seen to be opposite in trend to that for BVI noise levels, Fig. 12. This trend was also noted in Ref. 5. Still, however, with regard to the practicality of using 4P HHC for BVI noise reduction, this does not appear in itself to represent an overwhelming difficulty since the forces do not appear to increase over 10 to 20

removed for the present ARES data) would contribute to the loading transmitted to the fuselage. Depending on how the control system is designed, the net loading could either be increased or decreased.

Besides the forces in the fixed system, the blade root moments are important as an indication of dynamic rotor loads. Alternating flapwise blade bending moment data, in terms of 1/2 peak-to-peak values (not just the 4P component), are presented in Fig. 18. These data, compared to the 4P force data, also show minimum and maximum values at $\Psi_c=30^\circ$ and 60° , respectively, except at the higher μ values. There is more of a linear dependence of the flapwise moment with control amplitude θ_c than is found with the force data.

CONCLUSIONS

This study reveals the flight conditions where HHC can be used for BVI noise reduction and shows how the use of a 4P HHC affects the noise levels and vibratory loads. Mid-frequency noise reductions are higher (a maximum of 5.6 dB measured) at the lower speed descent conditions where BVI noise, without HHC, is most intense. No noise benefit is seen for flight conditions outside this range. The impulsive noise reductions correspond to reductions in blade pitch near the azimuth angle of about 60° where strong BVI is known to occur. There is some evidence that a blade-vortex displacement effect is an important factor in the noise reductions. Little can be said concerning the influence of vortex strength on the results. The use of 4P HHC produces increased low-frequency loading noise, but its effect, as based on subjective A-weighted (dBA) measure, is not relatively important when significant mid-frequency BVI noise reduction is attained. Also, vibratory loading increases, but the levels do not appear prohibitive in the low speed flight regime where one would consider using HHC for noise reduction. To the extent the increased vibration is a problem, the potential would seem to exist for HHC system design considerations to reduce vibration transmitted to the fuselage.

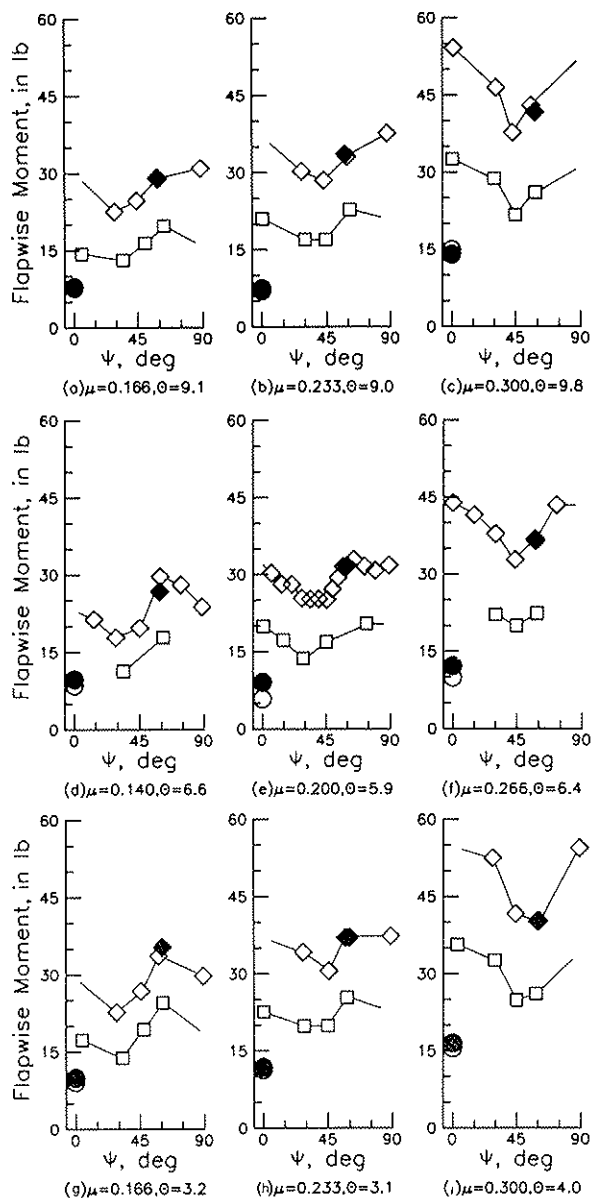


Fig. 18 Alternating flapwise bending moment (1/2 peak-to-peak), at 17 percent span, variation with different 4P HHC amplitudes and azimuth phases. Symbol key as in Fig. 12.

percent for operating conditions where HHC would actually be used, that is, for parts (d) and (e) of Figs. 12 and 17. It is also noted, that for a specific helicopter, HHC-control-system inertial terms (such as was

Aeroacoustic testing in heavy gas is demonstrated for the first time in this study. There appears to be no fundamental or practical difficulty in such testing or of scaling results to those one would obtain in air. In fact, a net scaling advantage is found for this study due to higher Reynolds numbers and dynamic scaling obtained through the use of heavy gas. With regard to the sound power approach it has been found to produce a useful quantitative spectral measure of the integrated noise field. The method, when applied properly, can be used with confidence when hard wall tunnel reflections prevent quality directivity measurements.

The use of HHC to reduce BVI noise appears to be a viable concept. One may envision the selective use of HHC to reduce subjective noise levels during helicopter landing approach, whereas otherwise its use during normal climb and cruise would be to reduce cabin vibration levels, as was its original purpose. It remains a task, however, to determine HHC schedules which maximize noise reduction and minimize the low-frequency noise and vibratory consequence of HHC use. The particular 4P HHC pitch schedule examined in this paper may very well prove to be a practical choice. However, other HHC schedules, which are possible for a four-bladed rotor with a conventional swashplate, that is, 3P, 5P, and any number of possible 3P-4P-5P mixed mode HHC schedules, should be carefully examined. The goal should be to minimize blade pitch motion and maximize the noise reduction benefit. The most desired control capability would be individual blade control (IBC), where the standard swashplate is eliminated. With IBC, the blade pitch schedules could be tailored to local azimuth regions, such as regions where tip vortices are shed and where the blade-vortex interactions occur. With either normal HHC or IBC, there is a question as to whether the most desired long range approach is open loop (prescribed, as was used here) or closed loop (iterative) control. This question can only be answered when more is known about the physics and predictability of the noise reduction mechanism. If the noise effects of HHC become sufficiently predictable for the important ranges of flight conditions, an open loop approach would appear best. However, if this is not the case, one would have to find representative microphone, and/or possibly blade surface pressure sensor, locations where measurements could be employed with adaptive closed-loop control system algorithms. A most important element of knowledge with regard to either approach is the noise directivity effects of HHC use, which are not addressable with the present data base.

ACKNOWLEDGMENTS

The authors would like to thank W. T. Yeager, Jr., M. L. Wilber, P. H. Mirick, and others in the Configuration Aeroelasticity Branch, LaRC, for rotor operation, TDT facility coordination, and extensive consultation. Appreciation is also extended to the Acoustic Measurement Group of Wyle Laboratories in Hampton, Virginia for high quality data acquisition support.

REFERENCES

1. J. C. Hardin, and S. L. Lamkin, "Concepts for Reduction of Blade/Vortex Interaction Noise," *J. Aircraft*, Vol. 24, No. 2, pp. 120-125, Feb 1987.

2. W. R. Spletstoesser, K. J. Schultz, and Ruth M. Martin, "Rotor Blade-Vortex Interaction Noise Source Identification and Correlation with Rotor Wake Predictions," AIAA 11th Aeroacoustics Conference, AIAA-87-2744, Oct. 1987.
3. E. R. Wood, R. W. Powers, and C. E. Hammond, "On Methods for Application of Harmonic Control," *Vertica*, Vol. 4, pp. 43-60, 1980.
4. T. F. Brooks, E. R. Booth, Jr., J. R. Jolly, Jr., W. T. Yeager, Jr., M. L. Wilbur, "Reduction of Blade-Vortex Interaction Noise Through Higher Harmonic Pitch Control," *J.A.H.S.*, Vol. 35, No. 1, pp. 86-91, Jan. 1990. (See also NASA TM-101624/AVSCOM TM 89-B-005, July 1989.)
5. W. R. Spletstoesser, G. Lehman, and B. van der Wall, "Higher Harmonic Control of a Helicopter Rotor to Reduce Blade-Vortex Interaction Noise," *Z. F. W. (Zeitschrift fur Flugwissenschaften)*, Vol. 14, pp. 109-116, 1990. (See also Proceedings of the 15th European Rotorcraft Forum, Sept. 1989)
6. W. R. Mantay, W. T. Yeager, Jr., M. N. Hamouda, R. G. Cramer, Jr., and C. W. Langston, "Aeroelastic Model Helicopter Rotor Testing in the Langley TDT," NASA TM-86440 (also USAAVSCOM TM-85-B-5), June 1985.
7. F. W. Schmitz, D. A. Boxwell, W. R. Spletstoesser, and K. -J. Schultz "Model Rotor High Speed Impulsive Noise: Full-Scale Comparisons and Parametric Variations," *Vertica*, Vol. 8, No. 4, pp. 395-422, 1984.
8. L. E. Kinsler and A. R. Frey, "Fundamentals of Acoustics," Chap. 9, Second Edition, John Wiley & Sons, Inc., New York, London, Sydney, 1962.
9. F. J. McHugh and J. Shaw, Jr., "Benefits of Higher-Harmonic Blade Pitch: Vibration Reduction, Blade-Load Reduction and Performance Improvement," Proceedings of the American Helicopter Society Mid-east Region Symposium on Rotor Technology, August 1976.
10. H. H. Heyson, "Use of Superposition in Digital Computers to Obtain Wind Tunnel Interference Factors for Arbitrary Configurations, with Particular Reference to V/STOL Models," NASA TR R-302, 1969.
11. T. F. Brooks, J. R. Jolly, and M. A. Marcolini, "Helicopter Main Rotor Noise—Determination of Source Contributions Using Scaled Model Data," NASA TP-2825, August 1988.